atmosphere

MDPI

Article

Diagnostic Ratios and Directional Analysis of Air Pollutants for Source Identification: A Global Perspective with Insights from Kuwait

Abdullah N. Al-Dabbous

Environment and Climate Change Program, Environment and Life Sciences Research Center, Kuwait Institute for Scientific Research, P.O. Box 24885, Safat 13109, Kuwait; adabbous@kisr.edu.kw

Abstract

Identifying the sources of atmospheric pollutants is essential for effective air quality management. This study assesses the diagnostic value of SO_2/NO_2 and CO/NO_2 ratios in distinguishing between major emission sources, including vehicular traffic, industrial activity, and biomass burning. A global literature review was conducted to establish typical ratio thresholds associated with different sources. These thresholds were then applied in a case study of Kuwait, a representative Gulf Cooperation Council country with intense vehicular traffic and industrial activity. To complement the ratio-based diagnostics, directional pollution source identification was performed using the Conditional Bivariate Probability Function (CBPF) plots, linking elevated pollutant concentrations to prevailing wind speeds/directions. Results indicate that Al-Fahaheel exhibits a distinct SO_2/NO_2 ratio toward the south-southeast due to industrial activities, and a pronounced CO/NO_2 ratio toward the east, reflecting contributions from mixed urban and traffic-related sources. The observed ratios at the Al-Fahaheel air quality monitoring station—very low CO/NO_2 and moderate to high SO_2/NO_2—are inconsistent with vehicular emissions and are more indicative of industrial emissions from stationary sources. Directional CBPF plots reinforce these associations by clearly linking industrial activities and vehicular traffic sources to the southeastern and western sectors, respectively.

Keywords: air pollution; source identification; SO_2/NO_2 ratio; CO/NO_2 ratio; directional analysis

check for updates

Academic Editor: Sunling Gong

Received: 7 August 2025
Revised: 10 September 2025
Accepted: 16 September 2025
Published: 18 September 2025

Citation: Al-Dabbous, A.N. Diagnostic Ratios and Directional Analysis of Air Pollutants for Source Identification: A Global Perspective with Insights from Kuwait. *Atmosphere* **2025**, *16*, 1101. https://doi.org/10.3390/atmos16091101

Copyright: © 2025 by the author. Licensee MDPI, Basel, Switzerland. This article is an open access article distributed under the terms and conditions of the Creative Commons Attribution (CC BY) license (https://creativecommons.org/licenses/by/4.0/).

1. Introduction

Air pollution poses a serious threat to public health, environmental sustainability, and global economic stability. Numerous studies have linked elevated concentrations of $PM_{2.5}$, PM_{10}, NOx, O_3, SO_2, and CO to the deterioration of air quality, and consequently, to adverse effects on human health and the environment in both outdoor [1,2] and indoor environments [3,4]. For instance, Chen and Hoek [5] demonstrated that long-term exposure to particulate matter, both $PM_{2.5}$ and PM_{10}, is significantly associated with increased mortality, including deaths from cardiovascular disease, respiratory illness, and lung cancer. Similarly, Huangfu and Atkinson [6] indicated that long-term exposure to NO_2 is associated with an increased risk of mortality from chronic obstructive pulmonary disease (COPD). Moreover, Orellano et al. [7] found that short-term exposure to ambient SO_2 is positively associated with increased risks of all-cause and respiratory mortality in humans. Additionally, Chen et al. [8] reported that both acute and chronic exposure to CO are

linked to an elevated risk of cardiovascular events, including mortality. Given the well-established health impacts associated with these pollutants, accurately identifying their sources is critical for guiding the development and implementation of effective air quality management policies.

In light of the severe health impacts of ambient air pollution outlined above, it is crucial to identify emission sources accurately and efficiently to mitigate pollutant levels. However, traditional receptor-based source apportionment methods (e.g., positive matrix factorization and principal component analysis) rely on detailed chemical speciation of PM for accurate source fingerprinting, which is often unavailable from routine monitoring stations. Similarly, source-based apportionment methods (e.g., dispersion modeling) require accurate emission inventories, which are often difficult and costly to obtain. As a practical alternative, researchers increasingly use diagnostic ratios and directional analysis of pollutants, based on routinely monitored data, to identify potential pollution sources. The ratios of sulfur dioxide to nitrogen oxides (SO_2/NOx) and carbon monoxide to nitrogen oxides (CO/NOx) have been widely used as qualitative fingerprints for distinguishing between emission types [9]. Different sources can be identified based on these pollutant ratios: a high CO/NOx ratio combined with a low SO_2/NOx ratio typically indicates emissions from mobile sources, whereas a low CO/NOx ratio and elevated SO_2/NOx ratio suggest contributions from stationary point sources [9]. These pollutant ratios have proven useful for source apportionment, particularly in the absence of detailed chemical speciation data for PM. Further threshold ranges of these diagnostic ratios, in association with specific source types, will be reviewed and established in Section 3.1. In parallel with the diagnostic ratio technique, the Conditional Bivariate Probability Function (CBPF) is a powerful method that integrates pollutant concentrations with prevailing wind speed and direction data to identify the likely pollution sources [10]. CBPF represents a step forward from earlier methods by combining the conventional Conditional Probability Function (CPF) with bivariate polar plots. By considering concentration intervals, CBPF enhances the ability to distinguish and characterize multiple emission sources at a monitoring site. The CBPF technique has been applied in a wide range of settings across North America, Europe, and Asia, demonstrating its broad usefulness in air quality management [10–13]. Accordingly, the present study leverages these techniques to identify the likely pollution sources.

The main objective of this study is to evaluate the use of SO_2/NO_2 and CO/NO_2 ratios, in combination with directional analysis, as effective tools for identifying air pollution sources. Three specific objectives are addressed to support this aim: Firstly, to review and summarize typical SO_2/NO_2 and CO/NO_2 ratio ranges reported in global literature and their associations with specific emission sources. These ratios will serve as reference benchmarks for future research, as the review brings together existing knowledge to support broader use in source identification studies. Secondly, to calculate and interpret these ratios using observed gaseous pollutant data from the Al-Fahaheel monitoring station in Kuwait for the years 2021–2022. Al-Fahaheel was selected as the case site due to its clear exposure to major pollution sources, including surrounding vehicular and industrial activities, as well as the availability of a Kuwait Environment Public Authority (KEPA)-operated air quality monitoring station. Thirdly, to apply the CBPF plots in order to determine the directional origin of key emission sources influencing air quality at the site. Although this study builds upon established analytical approaches, it adds value by integrating existing techniques to enhance source identification. To the best of our knowledge, no prior peer-reviewed studies have systematically applied directional analysis using CBPF or ratio-based source interpretation methodologies for air quality assessment in Kuwait or the broader Gulf Cooperation Council (GCC) region. The study provides reference ratio ranges for future

source diagnostics and highlights the effectiveness of combining them with directional analysis for source identification and, consequently, improved air quality management.

2. Methodology

2.1. Climate of Kuwait

Kuwait's climate is characterized by distinct seasonal fluctuations, particularly between summer and winter, with marked temperature and humidity variations throughout the year [14,15]. Winter (72 days) is marked by a significant drop in temperature, frequent cloud cover, occasional rainfall, and the dominance of very cold northwesterly winds. Spring (94 days) brings moderate but variable temperatures, with intermittent rain, thunderclouds, and hot southerly winds. Summer (168 days) is defined by a substantial rise in both temperature and humidity, resulting in prolonged periods of extreme heat. In Kuwait, the dominant wind direction is from the northwest, particularly during the dry summer months when northwesterly winds (known locally as "Semoom") prevail. The second most common wind direction is from the southeast (known locally as "Koos"), bringing humid air from the Arabian Gulf, especially during wet summer months. In contrast, autumn (31 days) features moderate temperatures, occasional cloud cover and rain, and notably cold nights. Kuwait experiences extreme seasonal variability in meteorological conditions, with summer temperatures reaching up to 53.0 °C (average: 36.4 °C) and relative humidity as high as 99.9% (average: 25.2%), while winter exhibits a broader temperature range (3.7–30.6 °C) and variable relative humidity (2.2–99.9%), reflecting the region's hot, arid, and wind-driven desert climate [14]. Further information on descriptive statistics and frequency distributions of Kuwait's meteorological parameters, including temperature, humidity, wind speed, and wind direction, can be found in Al-Dabbous et al. [14], and are also presented in Table 1.

Table 1. Seasonal Weather Characteristics in Kuwait.

Season [1]	Seasonal Phase	Duration	Days	Typical Weather Conditions	Dominant Wind Patterns
Winter	Cold	6 Dec–15 Jan	41	Cold weather with NW winds, warm weather intervals with wet SE winds	NW, SE
	Mild	16 Jan–15 Feb	31	Rain with SE winds, severe cold weather with NW winds	NW, SE
Spring	Cold moderate	16 Feb–8 April	52	Increase in temperature, hot S winds, and then moderate cold W winds, thunder, and dust storms	S, W, E (daytime), SE (daytime)
	Warm	9 April–20 May	42	More increase in temperature, humid and hot with SE winds, followed by NW winds, thunder, and dust storms	SE (morning), NW, E (afternoon)
Summer	Transition	21 May–5 Jun	16	Initiating summer with high temperatures and clear skies	Fluctuated
	Dry	6 Jun–19 Jul	44	Hot and dry with frequent dust storms	NW
	Wet	20 Jul–4 Nov	108	Hot and humid with light E and SE winds	E, SE
Autumn	-	5 Nov–5 Dec	31	Hot and humid with SE winds, cold (night) and warm (daytime)	SE, NW (at the end of the season)

[1] Seasonal information is based on the classification provided by the Directorate General of Civil Aviation (Meteorological Department), State of Kuwait [16].

2.2. Description of Study Area

In the GCC region, rapid urbanization, industrial growth, and a dependence on private vehicle transport have intensified local air pollution. Al-Fahaheel was selected as a representative example of a densely populated and high-activity urban area, characterized by intense industrial operations and traffic emissions. The study area, Al-Fahaheel, is located within the Al-Ahmadi Governorate in the southern region of Kuwait. It is a mixed-use urban zone that encompasses commercial, industrial, and residential developments [17–19]. Figure 1 shows the geographic context of Al-Fahaheel and the location of the air quality monitoring station. Geographically, Al-Fahaheel is surrounded by several key areas:

- **North**: Mangaf residential area.
- **South**: Major industrial zones including Mina Al-Ahmadi, Mina Al-Shuaiba, and Mina Abdullah.
- **East**: Arabian Gulf.
- **West**: Abdulaziz Bin Abdulrahman Al-Saud Expressway (Road 30).

Given Al-Fahaheel's proximity to several key pollution sources, the area experiences clear exposure to major emissions, allowing for distinct directional attribution to surrounding local sources. The total population of Al-Fahaheel is 106,839, which represents 9.2% of the Al-Ahmadi Governorate's population (1,160,096) and 2.1% of Kuwait's total population (5,098,539), according to the latest census published by the Public Authority for Civil Information (Issue No. 71, dated 30 June 2025). This population occupies 1861 buildings—equivalent to 3.6% of the total buildings in Al-Ahmadi Governorate (51,827)—comprising 1088 houses, 423 apartment buildings, and 350 other building types, distributed across 13 blocks.

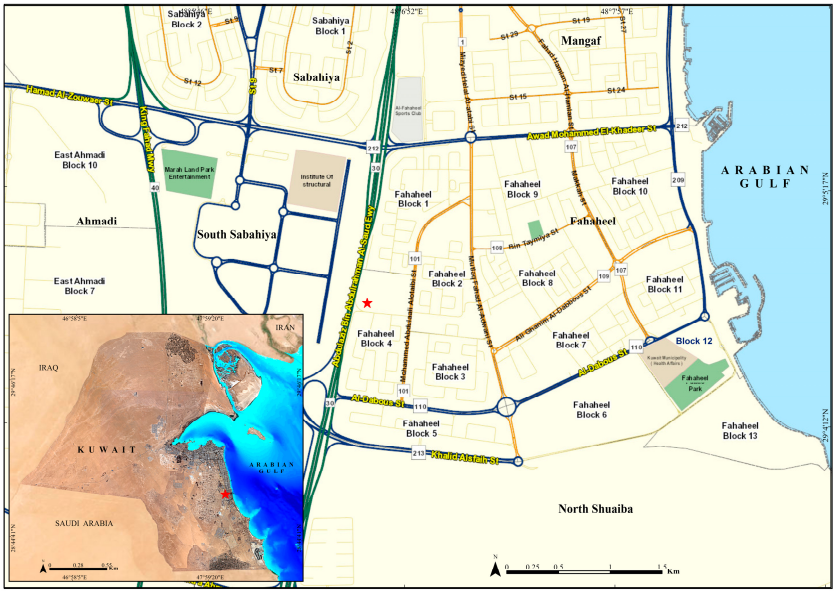


Figure 1. Study area of Al-Fahaheel, Kuwait, where the air quality monitoring station is marked with a red star symbol. The inset shows the broader geographic location of the study area within the State of Kuwait.

2.3. Data Acquisition/Interpretation

Hourly data of air pollutants were collected from the Al-Fahaheel air quality monitoring station for the period from 1 January 2021 to 31 December 2022. The Al-Fahaheel air quality monitoring station is operated and quality-controlled by KEPA, which was established in 2003. The focus on the two-year period (2021–2022) was primarily driven by data availability and quality assurance considerations, as this timeframe provided

consistent pollutant and meteorological records with minimal data gaps. The station is located at latitude 29.08032918 and longitude 48.11601436, positioned on the rooftop of the Fahaheel New Health Centre. It is situated on the western edge of the Al-Fahaheel residential area and lies approximately 200 m east of Abdulaziz Bin Abdulrahman Al-Saud Expressway (Road 30), a major highway in Kuwait. This strategic location allows the station to capture emissions from both nearby residential sources and high-traffic urban corridors. The station continuously monitors concentrations of key gaseous and particulate pollutants, providing essential data for regulatory assessment and scientific research. In this study, the monitored concentrations of SO_2 (ppb), CO (ppm), and NO_2 (ppb) were utilized for ratio-based diagnostics and directional source identification analyses. It should be noted, however, that while these ratios are effective for broadly distinguishing between mobile and stationary sources, they do not provide sufficient resolution to identify specific industrial types, which may vary regionally depending on fuels, processes, and emission control technologies. On the other hand, hourly meteorological data for the same period were collected from a nearby location operated and maintained by the Kuwait National Meteorological Network at the Kuwait Institute for Scientific Research (KNMN-KISR).

The collected air pollution and meteorological data were subsequently subjected to ratio-based diagnostics and directional analysis to identify the surrounding emission sources (vehicular and industrial sources). Specifically, SO_2/NO_2 and CO/NO_2 ratios were reviewed and evaluated to distinguish between major emission sources, such as vehicular and industrial sources, following the methodology described in Section 3.1. Given the limited vegetation cover and absence of significant biomass burning activity in Kuwait, contributions from this source are considered negligible under normal conditions and were therefore not further investigated in this study. However, biomass burning was briefly referenced in Section 3.1 as interpretive guidance, where literature-based ratio thresholds may assist researchers in future applications.

Bivariate polar plots were developed using the polarPlot function from the OpenAir package (version 2.18-2) in RStudio (version 4.2.2) to explore the directional dependence of pollutant concentrations on wind speed and wind direction. This function divides the data into wind speed-direction bins and computes the mean concentration within each bin [20]. Smoothing is applied to create a continuous surface; therefore, the color scale should be viewed as a general pattern, rather than exact values. The resulting polar plots provide a bivariate visualization that aids in identifying the directional influence of potential sources. Bivariate polar plots were developed for each of the studied pollutants (SO_2, CO, and NO_2), as well as for the derived ratios SO_2/NO_2 and CO/NO_2. Plotting polar plots of pollutant ratios helped reveal source patterns that were not visible in the individual pollutant polar plots.

To further support source identification, directional analysis was conducted using Conditional Bivariate Probability Function (CBPF) plots, allowing elevated pollutant concentrations to be associated with prevailing wind speeds and directions. The CBPF methodology applied in this study followed the approach detailed in Uria-Tellaetxe and Carslaw [10]. A total of 91 CBPF investigatory plots were initially prepared for each of the studied pollutants (SO_2, CO, and NO_2), taking into account wind speed, wind direction, and percentile intervals ranging from P0–P10, P1–P11, up to P90–P100. In some cases, adjacent percentile intervals were combined to improve source representation, particularly when elevated concentrations were distributed over similar directional sectors, thereby enhancing spatial clarity in the plots. From these plots, potential local sources were identified for each of the studied pollutants (SO_2, CO, and NO_2) across distinct percentile intervals, reflecting different concentration ranges, following the approach described by Uria-Tellaetxe and Carslaw [10].

3. Results and Discussion

3.1. Ratio Diagnostics in Literature: A Global Summary

Understanding the characteristic ratios of key pollutants can help identify the main emission sources contributing to air pollution in a given area. In particular, the ratios of SO_2/NOx and CO/NOx are commonly used as diagnostic indicators of different source types [9,21]. Different combustion sources emit these pollutants in distinct proportions due to variations in fuel sulfur content and combustion conditions [22,23]. Moreover, these ratios can vary significantly depending on the type of fuel used and the combustion technology utilized, which together determine combustion efficiency, temperature, air-fuel mixing, and emission profiles [24,25]. The following summary outlines the typical pollutant ratio signatures and key indicators associated with four major emission source categories, with Table 2 compiling literature-derived thresholds that aid in distinguishing these sources.

Table 2. Summary of SO_2/NOx and CO/NOx Ratios as Indicators of Pollution Sources.

Source Type	SO_2/NOx	CO/NOx	Key Indicators
Vehicular emissions	Very low	Moderate to high (variable)	Vehicular emissions are characterized by minimal sulfur content in their fuels, resulting in very low SO_2/NOx ratios. CO/NOx ratios in vehicular emissions can be (i) high (~50) in older or poorly tuned vehicles, (ii) moderate (~4–16) in modern urban fleets, and (iii) relatively low (~<1) in diesel engines, and in modern vehicular emissions with well-maintained engines or emission control technologies.
Industrial emissions	Moderate to high	Low	Industrial sources show low CO/NOx ratios due to efficient combustion processes designed for complete carbon oxidation. An SO_2/NOx ratio exceeding approximately 0.6 is suggested as a quantitative marker for industry-dominated air pollution, depending on source strength and emission control technologies. In heavy industries such as oil refineries, this ratio is often observed to exceed 1, reflecting the higher sulfur content of fuels and limited desulfurization.
Biomass burning emissions	Very low	Moderate to high	Biomass burning are characterized by minimal sulfur content in its fuels, resulting in very low SO_2/NOx ratios. Various types of biomass burning typically produce high CO/NOx ratios exceeding 15, indicating incomplete combustion. Both biomass burning and vehicular emissions exhibit high CO/NOx and low SO_2/NOx ratios, but they are distinguishable by their distinct temporal and spatial patterns.

Vehicular emissions: Vehicular emissions are typically characterized by high CO/NOx and low SO_2/NOx ratios [22], reflecting the incomplete combustion of gasoline or diesel in mobile sources and the low sulfur content in fuels, respectively. These emission profiles are prevalent in urban environments with dense traffic and low sulfur content in fuels [26]. A high CO/NOx ratio of approximately 50, as observed in urban New Delhi, is indicative of a dominant contribution from mobile vehicular emission sources, particularly in urban environments with older or poorly tuned engines [21]. Similarly, in Langkawi Island, Malaysia, high CO/NOx ratios ranging from 28.3 to 43.6 and low SO_2/NOx ratios between 0.04 and 0.12 were found to be indicative of vehicular emissions [27]. In line with this, for the period 1998 to 2000 at a road in downtown Delhi, the CO/NOx ratio was 81 and the SO_2/NOx ratio was 0.36 [28]. In Lahore, Pakistan, the CO/NOx and SO_2/NOx ratios were 9.72 and 0.07, respectively, reflecting the dominance of mobile sources [29]. Similarly, low SO_2/NOx ratios, with an interquartile range of 0.12–0.48 and mean values between

0.28 ± 0.19 and 0.47 ± 0.77, have been associated with traffic-related pollution [30]. On the other hand, diesel vehicles typically exhibit relatively lower CO/NOx ratios than gasoline vehicles; however, the average CO/NOx ratios for both vehicle types remain elevated relative to those from industrial sources [31]. This is evidenced by the low CO/NOx ratio of 0.8 observed in diesel-powered on-road vehicles, compared with a much higher ratio of 13.7 in gasoline-powered vehicles, as reported by Simon et al. [23]. This lower ratio in diesel engines (trailers and tankers) arises from their lean-burn combustion process, which emits less CO, and their higher in-cylinder temperatures, which promote greater NOx formation compared to gasoline engines [31,32]. CO/NOx ratios during morning traffic peaks in major U.S. cities ranged from approximately 5.7 in Nashville to 9.4 in Los Angeles. While there is some uncertainty in the absolute values due to potential biases, such biases are unlikely to affect long-term trends given the decadal scale of the study [33]. Similarly, Wallace et al. [34] reported CO/NOx ratios of 4.2 ± 0.6 during morning rush hours (05:00–09:00) and 5.2 ± 0.5 during daytime periods of highest traffic activity (08:00–18:00), indicating increased vehicular emissions associated with peak travel times. Air pollution in Kota Kinabalu, Malaysia, is predominantly influenced by mobile sources, as indicated by high CO/NO_2 ratios (80–140) and relatively low SO_2/NO_2 ratios (0.10–0.25) during weekdays [35]. Additional findings from another U.S. city reported CO/NOx ratios ranging from 7.8 ± 1.4 to 13.9 ± 2.4 during on-road traffic tunnel measurements in California [36]. During airborne mass balance experiments conducted by research aircraft around the Washington, D.C.–Baltimore area, the observed CO/NOx ratios were reported to be 4.6 for the University of Maryland aircraft and 5.1 for the C-130 aircraft [22].

Industrial emissions: Industrial emissions generally display low CO/NOx and high SO_2/NOx ratios due to the burning of sulfur-rich fuels such as heavy oil or coal in stationary sources [22], including power plants and petroleum refineries [37]. The low CO/NOx ratio in industrial emissions is primarily due to the low CO output from industrial combustion systems, which are typically designed to achieve near-complete fuel oxidation [38]. Based on Simon et al. [23], the CO/NOx ratio from oil and gas operations (ratio: 1.2) is significantly lower than that from gasoline-powered on-road vehicles (ratio: 13.7), reflecting more complete fuel oxidation in stationary sources. Elevated SO_2/NOx ratios arise because heavy oil and coal contain substantial sulfur that is released as SO_2 during combustion [39–41]. Emissions regulations implemented over the past two decades in many countries, such as the adoption of flue-gas desulfurization in power plants, have significantly reduced SO_2 emissions, thereby decreasing SO_2/NOx ratios in recent emission profiles [42]. Nevertheless, uncontrolled or older industrial sources and regions using high-sulfur fuels still exhibit elevated SO_2/NOx ratios. High SO_2/NOx ratios, with an interquartile range of 0.43–4.30 and mean values between 0.62 ± 0.61 and 7.01 ± 4.91, have been linked to industrial sources, with lower values typically associated with power plants and daytime emissions, and higher values indicating refinery activity under varying wind conditions [30]. Similarly, the SO_2/NO_2 ratio tends to be higher in regions with more developed industries that consume large amounts of sulfur-containing fuels [43]. A high SO_2/NO_2 ratio greater than 0.60 has been identified as a strong indicator of industrial sources in Jiangsu Province of China [41]. A similar SO_2/NOx ratio of 0.58 has been attributed to point source emissions in New Delhi, India [21]. Additionally, SO_2/NO_2 ratios across 27 Chinese provinces ranged from 1.02 to 4.98, further reflecting the substantial SO_2 emissions from industrial activities compared to NO_2 [39]. Based on a 16-year analysis (2005–2020) in China, SO_2/NO_2 ratios of 1.27 and 0.97 were attributed to emissions from ships and point sources (e.g., industrial processes), respectively [44].

Biomass burning emissions: Biomass burning emissions tend to exhibit varying (moderate to high) CO/NOx ratios, with generally low SO_2/NOx ratios depending on the type

of biomass and combustion conditions. These emissions are often linked to seasonal agricultural or wildfire burning activities and can vary depending on regional practices [45,46]. During the 2008–2009 period in India, field burning of crop residues resulted in significantly higher emissions of CO (65.98%) compared to SOx (0.35%), highlighting the dominance of incomplete combustion processes over sulfur-related emissions [47]. Various types of biomass burning (i.e., savanna and grassland, tropical forest, extratropical forest, biofuel burning, charcoal making, charcoal burning, and agricultural residues) typically produce high CO/NOx ratios exceeding 15, indicating incomplete combustion [45]. High CO/NOx ratios in biomass burning are indeed indicative of incomplete combustion typical of low-temperature smoldering [48]. In contrast, controlled or domestic biomass cooking fires typically yield relatively lower CO emissions, and thus lowering CO/NOx ratios, due to more efficient combustion practices [49–51]. SO_2/NOx ratios in biomass burning emissions are generally low due to the minimal sulfur content in most vegetative fuels [52]. While both biomass burning and vehicular emissions can show high CO/NOx and low SO_2/NOx ratios, they differ in temporal and spatial patterns. Biomass burning is seasonal, with peaks during dry periods or harvest seasons. In contrast, vehicular emissions are consistent throughout the year and typically peak during weekday urban rush hours.

3.2. Indicative Ratios for Pollution Sources in Kuwait

Figure 2 provides valuable insight into the spatial distribution of key pollutants (SO_2, CO, and NO_2) at the Al-Fahaheel air quality monitoring station during the period from 1 January 2021 to 31 December 2022, helping to explain the dominant emission sources in the area. The polar plot for SO_2 displays a clear hotspot toward the south-southeast at moderate wind speeds (around 5–10 m s^{-1}), indicating strong contributions from major industrial zones, including Mina Al-Ahmadi, Mina Al-Shuaiba, and Mina Abdullah. This pattern reflects emissions from refineries and power plants in these areas, which arise from the combustion of sulfur-rich fuels in stationary sources. This directional pattern coincides with the second most frequent wind direction in Kuwait (Section 2.1), which originates from the southeast, further supporting the attribution of SO_2 emissions to these stationary industrial sources. The polar plot for CO shows a pronounced hotspot toward the west at low wind speeds (around <5 m s^{-1}), corresponding to emissions from the nearby Abdulaziz Bin Abdulrahman Al-Saud Expressway (Road 30). This pattern highlights the significant impact of traffic-related emissions on local CO levels, reflecting the incomplete combustion of gasoline or diesel in mobile sources. The polar plot for NO_2 displays two prominent hotspots: one toward the west at low wind speeds, and another toward the south-southeast at slightly higher wind speeds. The western hotspot corresponds to emissions from Abdulaziz Bin Abdulrahman Al-Saud Expressway (Road 30), while the south-southeast hotspot reflects the influence of nearby industrial sources. Given that the prevailing wind direction in Kuwait is predominantly northwesterly (Section 2.1), particularly during the summer months, emissions from Road 30 are likely carried by these winds into the Al-Fahaheel area. This meteorological pattern enhances the impact of highway emissions on local air quality by facilitating the downwind transport of freshly emitted pollutants. This pattern underscores the combined impact of both mobile and stationary sources on local NO_2 concentrations.

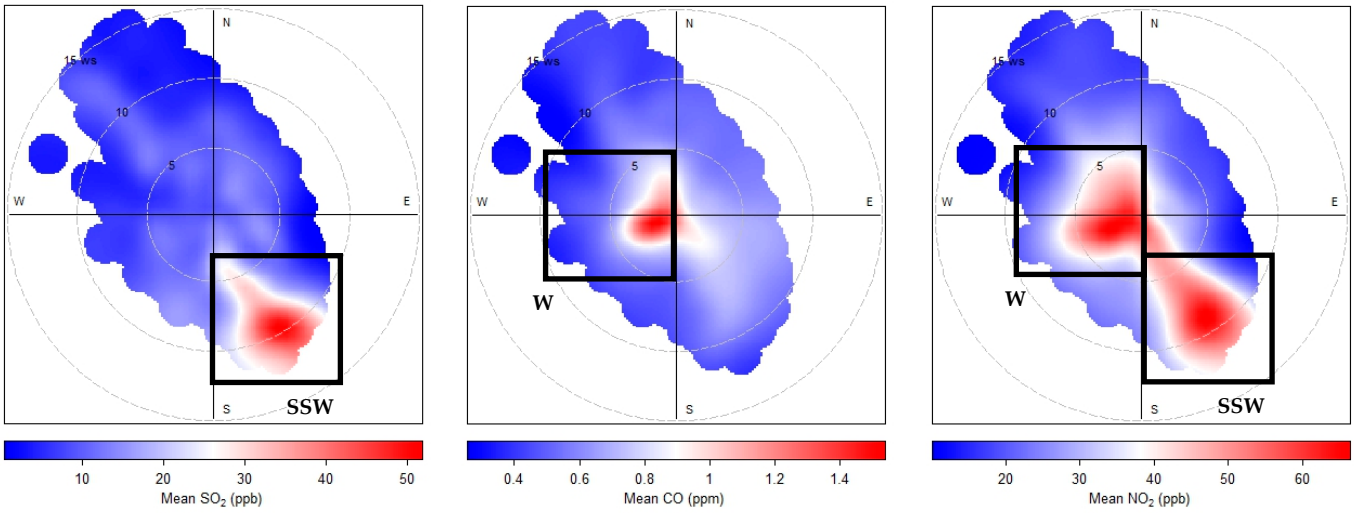


Figure 2. Bivariate polar plots for SO_2, CO, and NO_2 at Al-Fahaheel air quality monitoring station for the period from 1 January 2021 to 31 December 2022. The color scale in each panel represents the mean pollutant concentration across wind speed and wind direction bins. Red-shaded areas indicate higher concentrations and help reveal the directional influence of emission sources.

Figure 3 presents bivariate polar plots for SO_2/NO_2 and CO/NO_2 ratios at the Al-Fahaheel air quality monitoring station, covering the period from 1 January 2021 to 31 December 2022. These ratios are widely used as diagnostic indicators to distinguish between emission sources, since different combustion processes and fuel types result in characteristic relative emissions of these pollutants. The bivariate polar plot for SO_2/NO_2 reveals a distinct hotspot in the south-southeast direction at moderate wind speeds (approximately 5–10 m s^{-1}), coinciding with the second most frequent wind direction in Kuwait (Section 2.1), indicating significant contributions from industrial activities. This elevated ratio pattern is consistent with emissions from refineries and power plants burning sulfur-rich fuels, highlighting the dominant influence of stationary industrial sources on local sulfur-to-nitrogen pollutant dynamics. The bivariate polar plot for CO/NO_2 shows a distinct hotspot toward the east at moderate wind speeds (approximately 5–10 m s^{-1}), indicating an influence from mixed urban sources with varying combustion characteristics. This pattern reflects elevated relative CO emissions, potentially linked to incomplete combustion processes in those areas. Unlike Figure 2, which focuses on absolute CO concentrations and highlights the strongest emission areas directly (toward the west, due to heavy traffic), the bivariate polar plot for CO/NO_2 (Figure 3) emphasizes the relative abundance of CO compared to NO_2, revealing source differences and combustion conditions not evident in absolute concentration plots. The bivariate polar plot for CO/NO_2 (Figure 3) shows not only a distinct hotspot toward the east but also moderate (white-shaded) areas scattered in several directions, except for the south-southeast sector, where ratios remain consistently low. These scattered moderate ratios suggest contributions from mixed urban sources, possibly related to varying traffic densities. The absence of higher ratios in the south-southeast may indicate lower emissions or fewer contributing sources in that sector.

Following the literature-based diagnostic framework established in Section 3.1, the current section applies these pollutant ratios to the Al-Fahaheel dataset to characterize local emission source profiles based on observed concentration patterns. The SO_2/NO_2 ratio values at the Al-Fahaheel air quality monitoring station ranged from a minimum of 0.00004 to a maximum of 6.12, with a median of 0.20 and a mean of 0.31, indicating notable contributions from sulfur-rich industrial activities, such as oil-fired power plants, refineries, and heavy industries using high-sulfur fuels. In contrast, the CO/NO_2 ratio

values ranged from 0.00018 to 0.15, with a median of 0.02 and a mean of 0.022. These relatively low CO/NO_2 ratios are commonly associated with vehicular emissions involving well-maintained engines or emission control technologies, where efficient combustion processes result in lower CO output relative to NO_2. The consistently higher median, mean, and maximum values of SO_2/NO_2 compared to CO/NO_2 suggest a more significant influence from sulfur-rich combustion sources. In summary, the observed ratios—very low CO/NO_2 and moderate to high SO_2/NO_2—are inconsistent with vehicular emissions and are more indicative of industrial emissions from stationary sources.

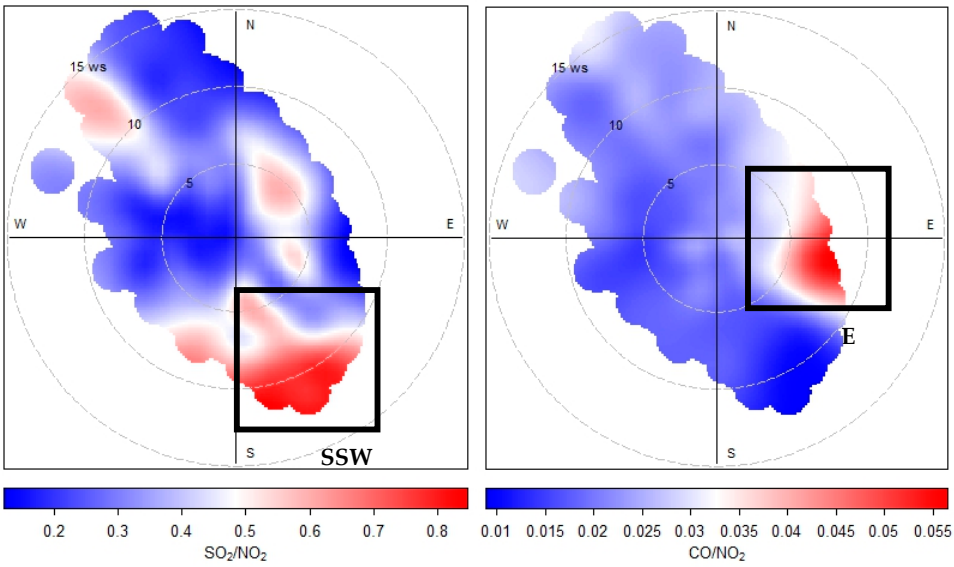


Figure 3. Bivariate polar plots for SO_2/NO_2, and CO/NO_2 at Al-Fahaheel air quality monitoring station for the period from 1 January 2021 to 31 December 2022. The color scale in each panel represents the ratio of the studied pollutants across wind speed and wind direction bins. Red-shaded areas indicate higher ratio values and help reveal the directional influence of emission sources.

3.3. Directional Source Identification in Kuwait Using CBPF Plots

This section presents the application of CBPF plots to identify the directional influence of local emission sources in Kuwait, providing spatial insight into the origin of elevated pollutant concentrations based on wind speed and direction following the approach described in Uria-Tellaetxe and Carslaw [10]. Figure 4 presents CBPF plots for selected percentile ranges, which are equivalent to concentration intervals, for (Figure 4a) SO_2 (16–271 ppb), (Figure 4b) CO (0.65–0.77 ppm), (Figure 4c) CO (0.77–5 ppm), (Figure 4d) NO_2 (17–22 ppb), and (Figure 4e) NO_2 (53–162 ppb) at the Al-Fahaheel air quality monitoring station for the period from 1 January 2021 to 31 December 2022. Only selected percentile ranges are presented in Figure 4 to avoid redundancy and emphasize clear, isolated source hotspots. Ranges with distinct directional hotspots and conditional probabilities above 0.6 were prioritized to ensure meaningful source interpretation. The red-shaded hotspots in these plots represent areas with the highest conditional probability of elevated pollutant concentrations under specific wind conditions, indicating strong directional source influence that coincides well with both prevailing wind directions in Kuwait—northwest and southeast (Section 2.1).

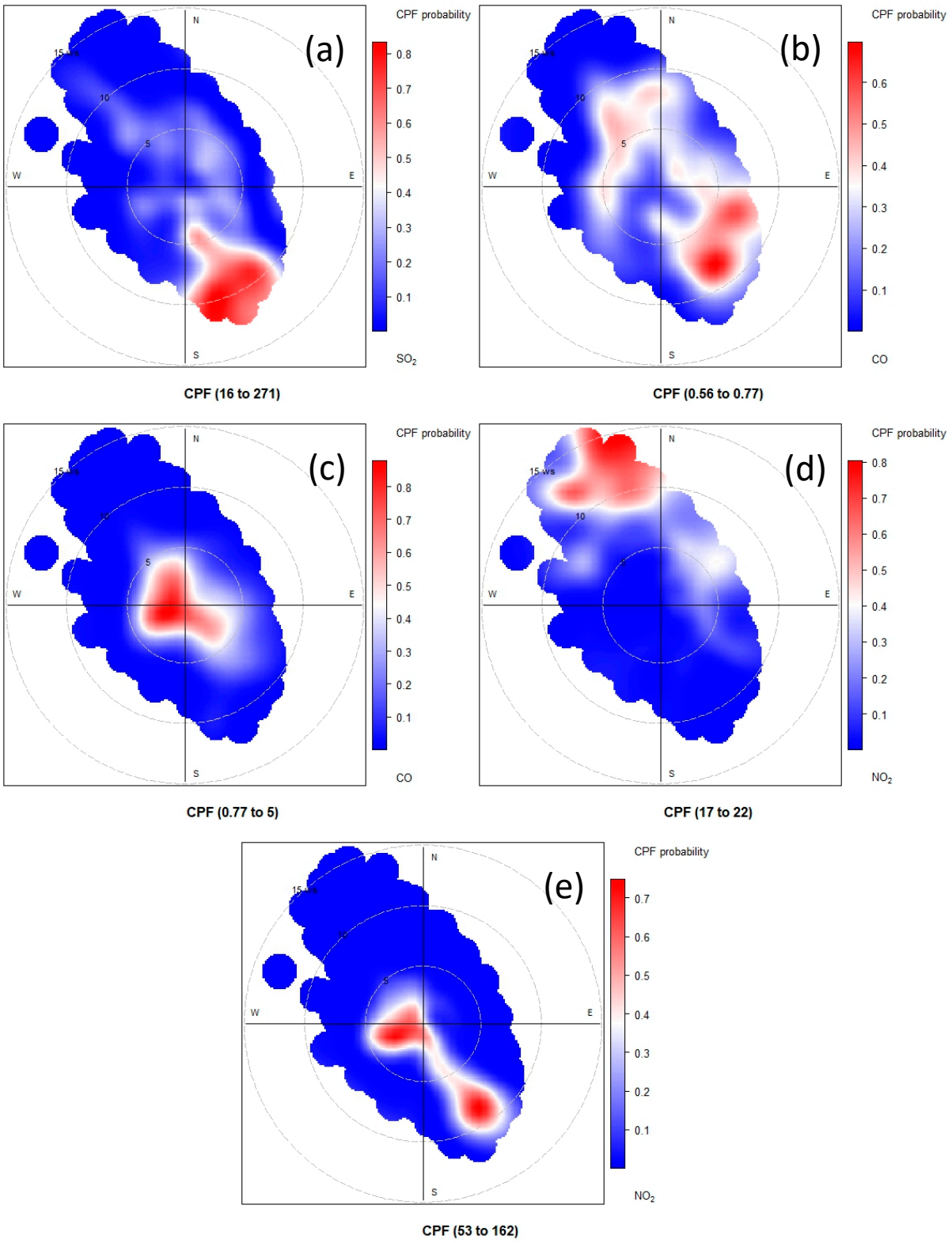


Figure 4. CBFP plots for selected percentile ranges (concentration intervals) for (**a**) SO_2 (16–271 ppb), (**b**) CO (0.65–0.77 ppm), (**c**) CO (0.77–5 ppm), (**d**) NO_2 (17–22 ppb), and (**e**) NO_2 (53–162 ppb) at Al-Fahaheel air quality monitoring station for the period from 1 January 2021 to 31 December 2022. The color scale in each panel represents the mean pollutant concentration within the specified percentile range across wind speed and wind direction bins. Red-shaded areas indicate higher concentrations and help identify the directional influence of emission sources.

Figure 4a illustrates the CBPF plot for SO_2 concentrations within the 80th to 100th percentile range (equivalent to 16–271 ppb), highlighting a distinct source influence from the south-southeast direction at moderate wind speeds (approximately 5–10 m s^{-1}). This directional pattern suggests a strong contribution from stationary industrial sources, likely associated with sulfur-rich fuel combustion in facilities such as refineries or power plants located in that sector.

The probable sources of CO are illustrated in Figure 4b,c, which represent CBPF plots for two percentile ranges: the 25th to 55th percentile (0.56–0.77 ppm) in Figure 4b, and the 55th to 100th percentile (0.77–5 ppm) in Figure 4c. In the lower concentration range (Figure 4b), a distinct source influence is observed in a similar direction to SO_2 (Figure 4a), suggesting contributions from stationary industrial sources. In contrast, the higher concentration range (Figure 4c) displays a pronounced hotspot toward the west at low wind speeds (approximately <5 m s^{-1}), indicating a dominant influence from nearby traffic emissions, particularly from Road 30. Together, these plots reflect the spatial variability of CO sources, with higher concentrations linked to localized traffic emissions and lower concentrations associated with industrial activities.

The probable sources of NO_2 are depicted in Figure 4d,e, representing two distinct percentile ranges: the 6th to 16th percentile (17–22 ppb) in Figure 4d and the 75th to 100th percentile (53–162 ppb) in Figure 4e. At the lower concentration range (Figure 4d), a clear hotspot appears toward the north-northwest at moderate to high wind speeds (approximately 10–15 m s^{-1}), potentially indicating regional background influence or long-range transport. In contrast, the higher concentration range (Figure 4e) displays two pronounced hotspots: one toward the west at low wind speeds (<5 m s^{-1}), consistent with traffic-related emissions from the nearby expressway (similar to Figure 4c), and another toward the south-southeast, associated with stationary industrial sources, in agreement with the spatial patterns observed for SO_2 (Figure 4a) and CO (Figure 4b). These results suggest that NO_2 concentrations in Al-Fahaheel are influenced by both mobile and stationary sources, with higher levels predominantly driven by local traffic and industrial activities.

4. Conclusions

The primary aim of this study was to review and assess the effectiveness of SO_2/NO_2 and CO/NO_2 ratios, alongside directional analysis, in identifying the dominant sources of air pollution, offering a global perspective supported by insights from the case of Kuwait. In general, vehicular and industrial emissions exhibited opposite ratio trends, with vehicular sources showing very low SO_2/NOx and variable CO/NOx ratios, while industrial sources displayed high SO_2/NOx and low CO/NOx ratios. Biomass burning generally shared similar ratio patterns to vehicular emissions but was distinguished by its unique temporal and spatial patterns. Nonetheless, the ratios applied here should be regarded as screening-level indicators of broad source categories. They are not sufficient to differentiate between distinct industrial types, which may vary across regions due to differences in fuel composition, combustion technology, and emission control measures. The methodology is therefore best applied as an initial diagnostic tool, to be complemented by more detailed receptor or source-based apportionment methods where available.

At the Al-Fahaheel air quality monitoring station, the pronounced SO_2 hotspot toward the south-southeast indicates dominant contributions from industrial sources, while the CO hotspot toward the west reflects traffic-related emissions from the nearby expressway, highlighting the contrasting impacts of stationary and mobile sources on local air quality based on absolute concentrations. Additionally, Al-Fahaheel data revealed clear signatures of industrial influence in the south-southeast sector, as evidenced by distinct SO_2/NO_2 ratios, and prominent contributions from traffic-related and mixed urban sources toward

the east, reflected in pronounced CO/NO_2 ratios. The observed ratios at the Al-Fahaheel air quality monitoring station—very low CO/NO_2 and moderate to high SO_2/NO_2—are inconsistent with vehicular emissions and are more indicative of industrial emissions from stationary sources. Directional analysis of the Al-Fahaheel air quality monitoring station using CBPF plots reinforced these findings by linking high pollutant levels to specific wind directions, effectively confirming local source contributions. The integration of ratio-based diagnostics with directional analysis provided a robust framework for source differentiation, even in environments lacking detailed chemical speciation data.

Future work should aim to extend the analysis across a longer temporal scale, subject to the availability of validated and continuous data. It is also recommended to conduct a more in-depth analysis of CBPF plots by exploring additional combinations of adjacent percentile ranges, which may enhance the identification and interpretation of overlapping or diffuse source contributions. Furthermore, it is recommended that future studies incorporate additional source identification techniques, such as seasonal variation analysis, temporal pattern evaluation, correlation, and cluster analysis, particularly when chemical speciation of particulate matter is unavailable for receptor-based source apportionment.

Funding: This research received no external funding.

Institutional Review Board Statement: Not Applicable.

Informed Consent Statement: Not Applicable.

Data Availability Statement: The original contributions presented in this study are included in the article. Further inquiries can be directed to the corresponding author.

Acknowledgments: The author gratefully acknowledges KEPA and KNMN-KISR for providing the air quality and meteorological data, respectively, used in this study. The author also wishes to thank Abeer Al-Saleh from the Environment & Life Sciences Research Center at KISR for assistance in preparing the map of the studied area.

Conflicts of Interest: The author declares no conflict of interest.

References

1. World Health Organization. *WHO Global Air Quality Guidelines: Particulate Matter (PM2. 5 and PM10), Ozone, Nitrogen Dioxide, Sulfur Dioxide and Carbon Monoxide*; World Health Organization: Geneva, Switzerland, 2021; ISBN 9789240034228.
2. Zhao, C.; Sun, Y.; Zhong, Y.; Xu, S.; Liang, Y.; Liu, S.; He, X.; Zhu, J.; Shibamoto, T.; He, M. Spatio-Temporal Analysis of Urban Air Pollutants throughout China during 2014–2019. *Air Qual. Atmos. Health* **2021**, *14*, 1619–1632. [CrossRef]
3. Amoatey, P.; Omidvarborna, H.; Baawain, M.S.; Al-Mamun, A. Indoor Air Pollution and Exposure Assessment of the Gulf Cooperation Council Countries: A Critical Review. *Environ. Int.* **2018**, *121*, 491–506. [CrossRef] [PubMed]
4. World Health Organization. *WHO Guidelines for Indoor Air Quality: Selected Pollutants*; World Health Organization: Geneva, Switzerland, 2010; ISBN 9789289002134.
5. Chen, J.; Hoek, G. Long-Term Exposure to PM and All-Cause and Cause-Specific Mortality: A Systematic Review and Meta-Analysis. *Environ. Int.* **2020**, *143*, 105974. [CrossRef] [PubMed]
6. Huangfu, P.; Atkinson, R. Long-Term Exposure to NO_2 and O_3 and All-Cause and Respiratory Mortality: A Systematic Review and Meta-Analysis. *Environ. Int.* **2020**, *144*, 105998. [CrossRef] [PubMed]
7. Orellano, P.; Reynoso, J.; Quaranta, N. Short-Term Exposure to Sulphur Dioxide (SO_2) and All-Cause and Respiratory Mortality: A Systematic Review and Meta-Analysis. *Environ. Int.* **2021**, *150*, 106434. [CrossRef]
8. Chen, T.-M.; Kuschner, W.G.; Gokhale, J.; Shofer, S. Outdoor Air Pollution: Nitrogen Dioxide, Sulfur Dioxide, and Carbon Monoxide Health Effects. *Am. J. Med. Sci.* **2007**, *333*, 249–256. [CrossRef]
9. Doğruparmak, Ş.Ç.; Özbay, B. Investigating Correlations and Variations of Air Pollutant Concentrations under Conditions of Rapid Industrialization–Kocaeli (1987–2009). *CLEAN Soil Air Water* **2011**, *39*, 597–604. [CrossRef]
10. Uria-Tellaetxe, I.; Carslaw, D.C. Conditional Bivariate Probability Function for Source Identification. *Environ. Model. Softw.* **2014**, *59*, 1–9. [CrossRef]

11. Althuwaynee, O.F.; Pokharel, B.; Aydda, A.; Balogun, A.-L.; Kim, S.-W.; Park, H.-J. Spatial Identification and Temporal Prediction of Air Pollution Sources Using Conditional Bivariate Probability Function and Time Series Signature. *J. Expo. Sci. Environ. Epidemiol.* **2021**, *31*, 709–726. [CrossRef] [PubMed]
12. Nguyen, T.N.T.; Vuong, Q.T.; Lee, S.-J.; Xiao, H.; Choi, S.-D. Identification of Source Areas of Polycyclic Aromatic Hydrocarbons in Ulsan, South Korea, Using Hybrid Receptor Models and the Conditional Bivariate Probability Function. *Environ. Sci. Process. Impacts* **2022**, *24*, 140–151. [CrossRef]
13. Sooktawee, S.; Kanabkaew, T.; Boonyapitak, S.; Patpai, A.; Piemyai, N. Characterising Particulate Matter Source Contributions in the Pollution Control Zone of Mining and Related Industries Using Bivariate Statistical Techniques. *Sci. Rep.* **2020**, *10*, 21372. [CrossRef] [PubMed]
14. Al-Dabbous, A.N.; Alsulaili, A.; Al-Dabbous, S.K. Description of Outdoor Air Quality in the Arabian Peninsula: A Case Study of Kuwait. In *Environmental Hazards in the Arabian Gulf Region. Advances in Natural and Technological Hazards Research*; Abd el-aal, A.e.K., Al-Enezi, A., Karam, Q.E., Eds.; Springer: Cham, Switzerland, 2024; Volume 54, pp. 265–284. ISBN 3-031-71836-4.
15. Alkhalidi, M.; Al-Dabbous, A.; Al-Dabbous, S.; Alzaid, D. Evaluating the Accuracy of the ERA5 Model in Predicting Wind Speeds Across Coastal and Offshore Regions. *J. Mar. Sci. Eng.* **2025**, *13*, 149. [CrossRef]
16. The Directorate General of Civil Aviation (Meteorological Department). Available online: https://www.met.gov.kw/Climate/climate.php?lang=eng#Annual_Report (accessed on 1 July 2025).
17. Al-Dabbous, A.; Khan, A.; Al-Rashidi, M.; Awadi, L. Carbon Dioxide and Volatile Organic Compounds Levels in Mosque in Hot Arid Climate. *Indoor Built Environ.* **2013**, *22*, 456–464. [CrossRef]
18. Al-Dabbous, A.N.; Kumar, P. Source Apportionment of Airborne Nanoparticles in a Middle Eastern City Using Positive Matrix Factorization. *Environ. Sci. Process. Impacts* **2015**, *17*, 802–812. [CrossRef]
19. Al-Salem, S.; Khan, A. Monitoring and Modelling the Trends of Primary and Secondary Air Pollution Precursors: The Case of the State of Kuwait. *Int. J. Chem. Eng.* **2010**, *2010*, 879836. [CrossRef]
20. Carslaw, D.C.; Ropkins, K. Openair—An R Package for Air Quality Data Analysis. *Environ. Model. Softw.* **2012**, *27*, 52–61. [CrossRef]
21. Aneja, V.P.; Agarwal, A.; Roelle, P.A.; Phillips, S.B.; Tong, Q.; Watkins, N.; Yablonsky, R. Measurements and Analysis of Criteria Pollutants in New Delhi, India. *Environ. Int.* **2001**, *27*, 35–42. [CrossRef]
22. Salmon, O.; Shepson, P.; Ren, X.; He, H.; Hall, D.; Dickerson, R.; Stirm, B.; Brown, S.; Fibiger, D.; McDuffie, E. Top-down Estimates of NOx and CO Emissions from Washington, DC-Baltimore during the WINTER Campaign. *J. Geophys. Res. Atmos.* **2018**, *123*, 7705–7724. [CrossRef]
23. Simon, H.; Valin, L.C.; Baker, K.R.; Henderson, B.H.; Crawford, J.H.; Pusede, S.E.; Kelly, J.T.; Foley, K.M.; Chris Owen, R.; Cohen, R.C. Characterizing CO and NOy Sources and Relative Ambient Ratios in the Baltimore Area Using Ambient Measurements and Source Attribution Modeling. *J. Geophys. Res. Atmos.* **2018**, *123*, 3304–3320. [CrossRef]
24. Sadeq, A.M.; Homod, R.Z.; Hasan, H.A.; Alhasnawi, B.N.; Hussein, A.K.; Jahangiri, A.; Togun, H.; Dehghani-Soufi, M.; Abbas, S. Advancements in Combustion Technologies: A Review of Innovations, Methodologies, and Practical Applications. *Energy Convers. Manag. X* **2025**, *26*, 100964. [CrossRef]
25. Sumarsono, D.A.; Agama, A.A.; Kurniawan, A.; Setiapraja, H. Performance, Emissions, and Combustion Analysis of Gasoline-Ethanol-Methanol Blends in a Spark-Ignition Engine. *Results Eng.* **2025**, *26*, 105264.
26. Garg, A.; Shukla, P.; Bhattacharya, S.; Dadhwal, V. Sub-Region (District) and Sector Level SO_2 and NOx Emissions for India: Assessment of Inventories and Mitigation Flexibility. *Atmos. Environ.* **2001**, *35*, 703–713. [CrossRef]
27. Halim, N.D.A.; Latif, M.T.; Ahamad, F.; Dominick, D.; Chung, J.X.; Juneng, L.; Khan, M.F. The Long-Term Assessment of Air Quality on an Island in Malaysia. *Heliyon* **2018**, *4*, e01054. [CrossRef]
28. Ravindra, K.; Wauters, E.; Tyagi, S.K.; Mor, S.; Van Grieken, R. Assessment of Air Quality after the Implementation of Compressed Natural Gas (CNG) as Fuel in Public Transport in Delhi, India. *Environ. Monit. Assess.* **2006**, *115*, 405–417. [CrossRef] [PubMed]
29. Haider, R.; Yasar, A.; Tabinda, A.B. Urban Emission Patterns at a Semi-Arid Site in Lahore, Pakistan. *Pol. J. Environ. Stud.* **2017**, *26*, 59–68. [CrossRef]
30. Nirel, R.; Dayan, U. On the Ratio of Sulfur Dioxide to Nitrogen Oxides as an Indicator of Air Pollution Sources. *J. Appl. Meteorol.* **2001**, *40*, 1209–1222. [CrossRef]
31. Ibeto, C.; Ugwu, C. Exhaust Emissions from Engines Fuelled with Petrol, Diesel and Their Blends with Biodiesel Produced from Waste Cooking Oil. *Pol. J. Environ. Stud.* **2019**, *28*, 3197–3206. [CrossRef]
32. Yasar, A.; Haider, R.; Tabinda, A.B.; Kausar, F.; Khan, M. A Comparison of Engine Emissions from Heavy, Medium, and Light Vehicles for CNG, Diesel, and Gasoline Fuels. *Pol. J. Environ. Stud.* **2013**, *22*, 1277–1281.
33. Parrish, D.D. Critical Evaluation of US On-Road Vehicle Emission Inventories. *Atmos. Environ.* **2006**, *40*, 2288–2300. [CrossRef]
34. Wallace, H.; Jobson, B.; Erickson, M.; McCoskey, J.; VanReken, T.; Lamb, B.; Vaughan, J.; Hardy, R.; Cole, J.; Strachan, S. Comparison of Wintertime CO to NOx Ratios to MOVES and MOBILE6. 2 on-Road Emissions Inventories. *Atmos. Environ.* **2012**, *63*, 289–297. [CrossRef]

35. Chang, J.H.W.; Chee, F.P.; Kong, S.S.K.; Sentian, J. Variability of the PM10 Concentration in the Urban Atmosphere of Sabah and Its Responses to Diurnal and Weekly Changes of CO, NO2, SO2 and Ozone. *Asian J. Atmos. Environ.* **2018**, *12*, 109–126. [CrossRef]
36. Fujita, E.M.; Campbell, D.E.; Zielinska, B.; Chow, J.C.; Lindhjem, C.E.; DenBleyker, A.; Bishop, G.A.; Schuchmann, B.G.; Stedman, D.H.; Lawson, D.R. Comparison of the MOVES2010a, MOBILE6. 2, and EMFAC2007 Mobile Source Emission Models with on-Road Traffic Tunnel and Remote Sensing Measurements. *J. Air Waste Manag. Assoc.* **2012**, *62*, 1134–1149. [CrossRef] [PubMed]
37. Krotkov, N.A.; McLinden, C.A.; Li, C.; Lamsal, L.N.; Celarier, E.A.; Marchenko, S.V.; Swartz, W.H.; Bucsela, E.J.; Joiner, J.; Duncan, B.N. Aura OMI Observations of Regional SO 2 and NO 2 Pollution Changes from 2005 to 2015. *Atmos. Chem. Phys.* **2016**, *16*, 4605–4629. [CrossRef]
38. Li, P.; Zhuo, Y.; Feng, C.; Hu, P. Effects of Interfering Gases on Catalytic Oxidation of Carbon Monoxide over Manganese Dioxide in Industrial Scenarios: A Systematic Study. *Mol. Catal.* **2024**, *565*, 114362. [CrossRef]
39. Ali, M.A.; Assiri, M.E.; Islam, M.N.; Bilal, M.; Ghulam, A.; Huang, Z. Identification of NO2 and SO2 over China: Characterization of Polluted and Hotspots Provinces. *Air Qual. Atmos. Health* **2024**, *17*, 2203–2221. [CrossRef]
40. Filonchyk, M.; Peterson, M.P. An Integrated Analysis of Air Pollution from US Coal-Fired Power Plants. *Geosci. Front.* **2023**, *14*, 101498. [CrossRef]
41. Wang, Y.; Ali, M.A.; Bilal, M.; Qiu, Z.; Mhawish, A.; Almazroui, M.; Shahid, S.; Islam, M.N.; Zhang, Y.; Haque, M.N. Identification of NO2 and SO2 Pollution Hotspots and Sources in Jiangsu Province of China. *Remote Sens.* **2021**, *13*, 3742. [CrossRef]
42. Zheng, B.; Tong, D.; Li, M.; Liu, F.; Hong, C.; Geng, G.; Li, H.; Li, X.; Peng, L.; Qi, J. Trends in China's Anthropogenic Emissions since 2010 as the Consequence of Clean Air Actions. *Atmos. Chem. Phys.* **2018**, *18*, 14095–14111. [CrossRef]
43. Zhao, P.; Tuygun, G.T.; Li, B.; Liu, J.; Yuan, L.; Luo, Y.; Xiao, H.; Zhou, Y. The Effect of Environmental Regulations on Air Quality: A Long-Term Trend Analysis of SO_2 and NO_2 in the Largest Urban Agglomeration in Southwest China. *Atmos. Pollut. Res.* **2019**, *10*, 2030–2039.
44. Ali, M.A.; Wang, Y.; Bilal, M.; Assiri, M.E.; Islam, A.R.M.T.; Malafaia, G.; Huang, Z.; Mhawish, A.; Islam, M.N.; Qiu, Z. Trace Gases over Land and Ocean Surfaces of China: Hotspots, Trends, and Source Contributions. *Earth Syst. Environ.* **2023**, *7*, 801–819. [CrossRef]
45. Andreae, M.O.; Merlet, P. Emission of Trace Gases and Aerosols from Biomass Burning. *Global Biogeochem. Cycles* **2001**, *15*, 955–966. [CrossRef]
46. Streets, D.G.; Bond, T.; Carmichael, G.; Fernandes, S.; Fu, Q.; He, D.; Klimont, Z.; Nelson, S.; Tsai, N.; Wang, M.Q. An Inventory of Gaseous and Primary Aerosol Emissions in Asia in the Year 2000. *J. Geophys. Res. Atmos.* **2003**, *108*, 8809. [CrossRef]
47. Jain, N.; Bhatia, A.; Pathak, H. Emission of Air Pollutants from Crop Residue Burning in India. *Aerosol Air Qual. Res.* **2014**, *14*, 422–430. [CrossRef]
48. Chen, L.-W.A.; Moosmüller, H.; Arnott, W.P.; Chow, J.C.; Watson, J.G.; Susott, R.A.; Babbitt, R.E.; Wold, C.E.; Lincoln, E.N.; Hao, W.M. Emissions from Laboratory Combustion of Wildland Fuels: Emission Factors and Source Profiles. *Environ. Sci. Technol.* **2007**, *41*, 4317–4325. [CrossRef] [PubMed]
49. Akagi, S.; Yokelson, R.J.; Wiedinmyer, C.; Alvarado, M.J.; Reid, J.S.; Karl, T.; Crounse, J.D.; Wennberg, P.O. Emission Factors for Open and Domestic Biomass Burning for Use in Atmospheric Models. *Atmos. Chem. Phys.* **2011**, *11*, 4039–4072. [CrossRef]
50. Bentson, S.; Evitt, D.; Still, D.; Lieberman, D.; MacCarty, N. Retrofitting Stoves with Forced Jets of Primary Air Improves Speed, Emissions, and Efficiency: Evidence from Six Types of Biomass Cookstoves. *Energy Sustain. Dev.* **2022**, *71*, 104–117. [CrossRef]
51. Hayyat, U.; Khan, M.U.; Farooq, M.; Sultan, M.; Amjed, M.A.; Liu, G.; Chunyu, X.; Riaz, F.; Alkhedher, M. Recent Developments and Challenges in Biomass Cookstove. *Energy Rep.* **2024**, *12*, 2193–2208. [CrossRef]
52. Vakkilainen, E.K. Industrial Applications of Steam Generated from Biomass. In *Comprehensive Renewable Energy*; Elsevier: Amsterdam, The Netherlands, 2022; pp. 299–329. ISBN 978-0-12-819734-9.

Disclaimer/Publisher's Note: The statements, opinions and data contained in all publications are solely those of the individual author(s) and contributor(s) and not of MDPI and/or the editor(s). MDPI and/or the editor(s) disclaim responsibility for any injury to people or property resulting from any ideas, methods, instructions or products referred to in the content.